IEEE Access
Multidisciplinary | Rapid Review | Open Access Journal

Received May 10, 2019, accepted May 25, 2019, date of publication May 30, 2019, date of current version June 19, 2019.

Digital Object Identifier 10.1109/ACCESS.2019.2920103

Unmanned Aerial Vehicle-to-Wearables (UAV2W) Indoor Radio Propagation Channel Measurements and Modeling

AMIT KACHROO[1], (Student Member, IEEE), SURBHI VISHWAKARMA[1], JACOB N. DIXON[2], (Student Member, IEEE), HISHAM ABUELLA[1], (Student Member, IEEE), ADITHYA POPURI[1], QAMMER H. ABBASI[3], (Senior Member, IEEE), CHARLES F. BUNTING[1], (Fellow, IEEE), JAMEY D. JACOB[4], AND SABIT EKIN[1], (Member, IEEE)

[1]School of Electrical and Computer Engineering, Oklahoma State University, Stillwater, OK 74078, USA
[2]IBM, Rochester, MN 55901, USA
[3]School of Engineering, University of Glasgow, Glasgow G12 8QQ, U.K.
[4]School of Mechanical and Aerospace Engineering, Oklahoma State University, Stillwater, OK 74078, USA

Corresponding author: Amit Kachroo (amit.kachroo@okstate.edu)

ABSTRACT In this paper, off-body ultra-wide band (UWB) channel characterization and modeling are presented between an unmanned aerial vehicle (UAV) and a human subject. The wearable antenna was patched at nine different body locations on a human subject during the experiment campaign. The prime objective of this work was to study and evaluate the distance and frequency dependent path loss factors for different bandwidths corresponding to various carrier frequencies, and also look into the time dispersion properties of such unmanned aerial vehicle-to-wearables (UAV2W) system. The environment under consideration was an indoor warehouse with highly conductive metallic walls and roof. Best fit statistical analysis using Akaike Information Criteria revealed that the Log-normal distribution is the best fit distribution to model the UWB fading statistics. The study in this paper will set up a road map for future UAV2W studies to develop enhanced retail and remote health-care monitoring/diagnostic systems.

INDEX TERMS Ultra-wide band, unmanned aerial vehicle, off-body channel modeling, time dispersion parameters, path gain, path loss.

I. INTRODUCTION

In recent years, unmanned aerial vehicles (UAVs) are considered to be the next frontier in technology advancement especially in the retail, defense and health care sectors [1]–[3]. In retail, UAVs are being utilized to do warehouse operations such as inventory management, stock counting by RF tagging or by using computer vision. The main advantage of utilizing UAVs for such operations is that it is far more time efficient than human and forklift trucks [4], [5]. Although the pick and drop of items capability is still limited but in future that would not be a limitation anymore given the advancements in drone technology, IoT, and machine learning over the years. Another application of UAV is the remote health-care in crowded or far-flung areas with no accessibility [1] or in case of emergency like cardiac arrest [6] where drones can be used to send life saving drugs. The other important application is the direct health care monitoring from a UAV to the wearable device that is attached to a patient body. This type of system is referred in this paper as unmanned aerial vehicle-to-wearable (UAV2W) systems. The remote health-care delivery by drones has been a topic of study for long [1], [6]–[8] but the study of UAV2W systems considering ultra-wide band channels and a human subject was missing. Thus the need to do exhaustive measurement campaign, and to study these type of systems were very much required which this study tries to fulfill.

Apart from UAVs, the ultra-wide band (UWB) technology has also attracted a lot of attention not only from the academia but also from the industry as well. The main reasons behind its popularity is the low-power consumption and high bandwidth with low probability of interception [9]–[12]. The low

The associate editor coordinating the review of this manuscript and approving it for publication was Akram Alomainy.

power consumption and short wavelength makes the UWB as a best possible candidate for the body-centric wireless network [13], [14] in health-care applications [10], [11]. The Federal Communication Commission's (FCC) power requirement of −41.3 dBm/Mhz or 75 nanowatts/Mhz classifies UWB as an unintentional radiators which allows it to lie below the noise floor for a narrowband receiver and thereby can easily coexist with current wireless technologies like WiFi with minimal or no interference. Recent literature points out bundle of UWB radio channel characteristics campaigns done for on-body and off-body scenarios. In [12], [15]–[20], on-body UWB radio channel characterization and modeling were investigated in detail. However, most of the research on off-body radio channel has a controlled environment, where antennas are placed in standalone position. In [21], [22], UWB radio channel modeling for UAV is presented without a real human subject. The closest research to our work is presented in [9], [10], where the off- and on-body channel characterization were performed. The main difference with these work is that we have considered the UWB radio channel between a UAV and a human subject in our work.

As per author's knowledge, this is the first work to consider such a scenario for UWB channel characterization domain. The contribution of this paper can be summarized as:

- Distance dependent and frequency dependent path loss factor for different bandwidth with corresponding carrier frequency is studied and determined in detail.
- Time dispersion properties such as root mean square delay, mean excess delay and maximum excess delay in UAV2W systems is evaluated and found for different body locations.
- Log-normal distribution was found to be the best fit distribution for large scale fading statistics which was confirmed by Akaike Information Criterian.

The rest of the paper is as follows, Section II discusses about the measurement setup and data acquisition part, Section III covers the radio channel characterization, Section IV looks at the statistical modeling part and finally, Section V presents the conclusion.

II. MEASUREMENT SETUP AND DATA ACQUISITION

In this section, the vector network analysis (VNA) based measurement set up will be described in detail. Fig. 1 shows the measurement set up where the transmitter (Tx) antenna was patched on a UAV while the wearable receiver (Rx) antenna was patched on a human subject. Both Rx antenna and Tx antenna were connected to the vector network analyzer (VNA) on port 1 and port 2 respectively. The transmit power was set at -40 dB to make the UWB power exist near the noise floor at wideband frequencies. One important observation here is that the noise floor changes with the bandwidth and the relationship between noise floor and bandwidth is given as,

$$\text{Noise floor (dBm)} = 10\log_{10}(kT) + 10\log_{10}(B) + NF, \quad (1)$$

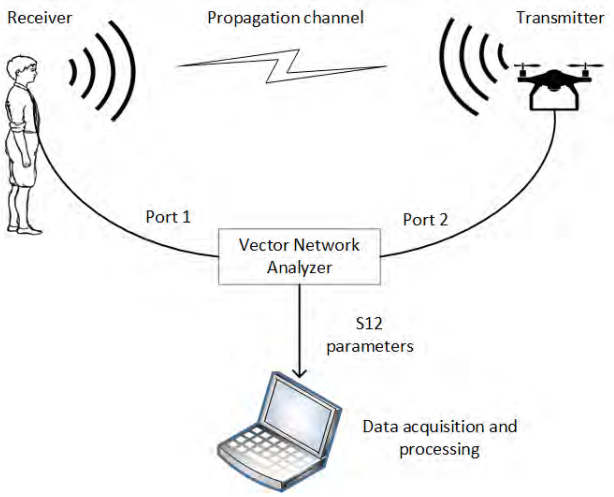

FIGURE 1. The UAV2W experiment setup with data acquisition and processing component.

where k is the Boltzmann's constant, T is the temperature of receiver system in Kelvins, NF is the noise figure of receiver and B is the given bandwidth. Therefore, in our set up, given the FCC regulations and the human subject involved, the transmit power of -40 dB was considered to be sufficient transmit power. Also, no power amplifier was used in transmission path as is generally the case that doesn't involve human subject to take care of the regulations and human subject.

The VNA was further set up with the sweep time of 100 ms (milliseconds) to generate 1601 continuous wave tones that were uniformly distributed over the frequency range of 3.1-10.6 GHz; this frequency range is widely accepted for ultra wide band related measurements. The VNA was then calibrated to remove the cable effects which in indoor and small distances is manageable as compared to outdoor environment and over long distance in UWB. The measurement data (S12 parameter) thus collected will be the channel transfer function in frequency domain. The S12 parameters were acquired and processed by Python and MATLAB scripts on a laptop. The data analysis was done on this recorded data set to find the UWB distance dependent and frequency dependent path loss factors and time dispersion parameters like root mean square time, maximum excess time that will be discussed in next section.

The list of equipment with their individual specifications used in the measurement process are listed in Table 1. The UWB antenna patch (Octane BW-3000-10000-EG [23]) is an Omni-directional wideband antenna with 5.5 dBi gain at 3 GHz, 8.2 dBi gain at 6 GHz and 6.3 dBi gain at 9 GHz. It is lightweight (2 ounces) and small in dimensions ($4.5'' \times 4.25'' \times 0.4''$) with voltage standing wave ratio (VSWR) less than 2:1. On the other hand, the UAV (IRIS+ quadcopter) has the maximum speed of 25 mph with 3 DR link communication [24]. The Octave antenna and IRIS+ quadcopter used in this study are shown in Fig. 2. The 9 different

TABLE 1. The measurement equipment with the specifications.

Equipment	Specifications
Vector Network Analyzer	Agilent 8722ES (50 MHz-40 GHz)
Calibration kit	Agilent 85032F
UAV	3 DR IRIS + Quadcopter
RF coaxial cables	Weight 2 lbs
2 Antenna sensors	OctaneBW-3000 (3 GHz-11 GHz)

FIGURE 2. Octane antenna and IRIS+ quadcopter.

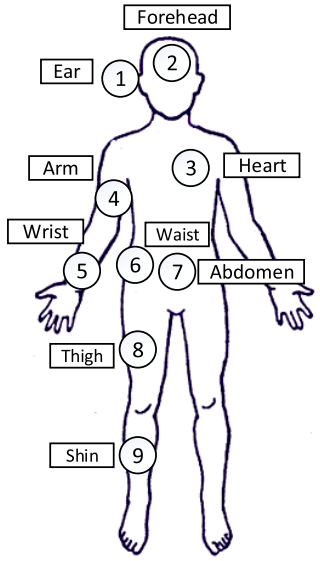

FIGURE 3. The UWB antenna patch locations on human body for line-of-sight (LOS) measurements in the indoor warehouse scenario.

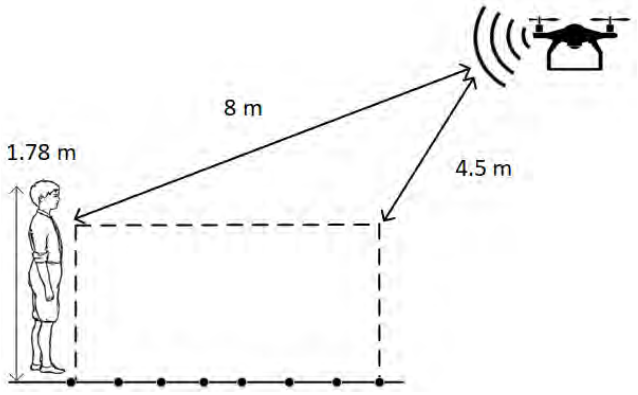

FIGURE 4. The sketch plan of the measurement setup for UWB off-body characterization with 8 points marked on the ground. The farthest diagonal distance was 8 m while the nearest was 4.5 m towards the UAV.

body locations where the UWB antenna (Rx) was placed is shown in Fig. 3.

On the other hand, the transmitter antenna was fixed on the UAV that was hovering at a fixed height. The human subject (receiver) moved 0.5 meter from one point to another on the ground (8 points in total) covering a diagonal range of 8.0 meter to 4.5 meters towards the UAV. The complete sketch plan with the 8 marked points on the ground and with the farthest and nearest diagonal distance between UAV and the human subject is shown in Fig. 4

At each distance point and for a specific body location, a total of 10 snapshots of the data (S12) were recorded which were later on averaged[1] to get a better redundant value. The time domain response from these frequency response measurements was computed by taking the Inverse Fast Fourier Transform (IFFT), which will be discussed in detail in the next section. Fig. 5 shows the actual indoor warehouse environment where this measurement campaign was carried out. In the next section, we will dwell more into the data analysis part.

III. UWB-UAV2W RADIO CHANNEL CHARACTERIZATION

In this section, first analysis for the path gain modeling at different bandwidth corresponding to several frequency carriers will be carried out and then the time dispersion analysis for UAV2W systems will be discussed in detail from the S12-data collected as mentioned in previous section.

[1]It is very important to note that the averaging was done on linear scale not on the recorded dB scale of the VNA.

FIGURE 5. Indoor warehouse environment for the campaign.

A. PATH GAIN ANALYSIS

The detailed path gain calculation for a UWB system is provided in these exceptional work of [25]–[27]. The distance dependent path gain[2] is well known to follow a log-distance model in which linear curve fitting is done to determine the path loss exponents. However, the interesting part is that at the UWB frequencies the path loss is not just distance dependent but also frequency dependent [26], [27].

The total path gain PG(f, d) as a function of distance and frequency assuming that the distance dependent path gain and frequency dependent path gain are independent [25], [27], [28] is given as,

$$\mathrm{PG}(f, d) = \mathrm{PG}(f) \cdot \mathrm{PG}(d). \tag{2}$$

The distance dependent path gain PG(d) is modelled with the power law relationship while frequency dependent path gain PG(f) is modelled as: PG$(f) \propto f^{-k}$, where k denotes the frequency dependent path loss factor. Therefore the total path gain is given as [26],

$$\mathrm{PG}_{dB}(f, d) = \overline{\mathrm{PG}}_{dB}(f_c, d_0) - 10n \log_{10}\left(\frac{d}{d_0}\right) - 20k \log_{10}\left(\frac{f}{f_c}\right) + X_\sigma(d), \tag{3}$$

where d is the distance between Tx and Rx, f is the frequency under consideration, $\mathrm{PG}_{dB}(f_c, d_0)$ is the mean of $\overline{\mathrm{PG}}_{dB}(f_c, d_0)$ at a reference distance $d_0 = 1\ m$, and at the reference frequency $f_c = 1$ GHz. Also, n is the distance dependent path loss exponent, k is the frequency dependent exponent and $X_\sigma(d)$ is the shadowing factor which is Gaussian distributed with zero mean (in dB) and a variance of σ^2 (in dB).

[2]Path gain is described as the ratio of received power to the transmitted power while path loss is the inverse of path gain that is (PL_{dB} =-PG_{dB}).

TABLE 2. Frequency bandwidth with different carrier frequency.

BW (GHz)	Frequency carrier (f_c (GHz)
0.75	3.47, 4.22, 4.97, 5.72, 6.47, 7.22, 7.97, 8.72, 9.47
1.5	3.85, 5.35, 6.85, 8.35, 9.85
3	4.60, 6.85, 9.10
3.75	4.97, 8.72
7.5	6.85

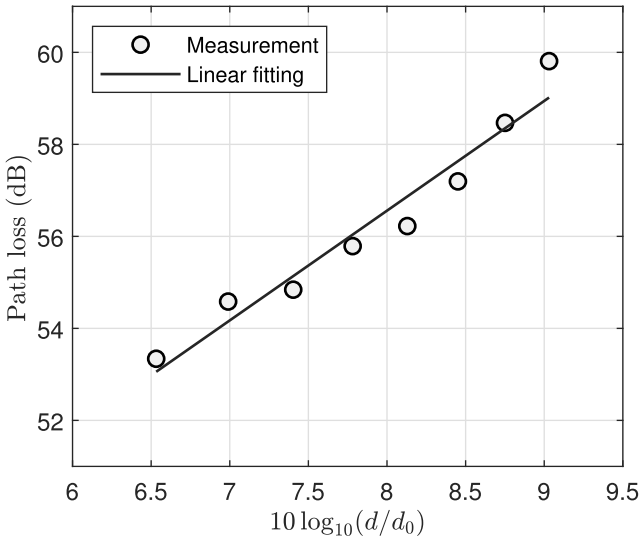

FIGURE 6. Linear fitting to determine the distance dependent path loss factor (n) between Forehead location of the human subject and UAV.

Moreover, in order to analyze the distance dependent and frequency dependent path loss exponent over different frequency bands, the UWB spectrum was divided into different bandwidths with different set of frequency carriers associated with it [25]. Table 2 shows the different frequency carrier set with the different bandwidths of 0.75, 1.5, 3.0, 3.75, 7.5 GHz. Therefore, for each bandwidth there will be different path loss exponent corresponding to the various frequency carriers, for example at 3.0 GHz bandwidth there will be three path loss exponents corresponding to the three frequency carriers of 4.6, 6.85 and 9.1 GHz.

Now, to calculate the distance dependent S12 parameter, we need to average it over all the frequency tones and similarly to determine the frequency dependent S12 parameter, we need to average it over all the distance. Therefore, using mean square error method, the S12 at a distance d and f is given as:

$$\mathrm{S12}_{dB}(d) = 10\log_{10}\left(\frac{1}{M}\sum_{j=1}^{M}\frac{1}{N}\left[\sum_{i=1}^{N}|H(t_i, f_j, d)|^2\right]\right),$$
$$\mathrm{S12}_{dB}(f) = 20\log_{10}\left(\frac{1}{L}\sum_{p=1}^{L}\frac{1}{N}\left[\sum_{i=1}^{N}|H(t_i, f, d_p)|^2\right]\right), \tag{4}$$

where $N = 10$ are the 10 snapshots at each frequency tone and $M = 1601$ are the 1601 frequency tones (frequency sweep points from 3.1 GHz to 10.6 GHz), L are the 8 distance

TABLE 3. Distance dependent path loss factor (n) and frequency path loss factor (k) for different bandwidths corresponding to various carrier frequencies (f_c) for UAV2W systems.

Loss factor	BW (GHz)	Carrier frequency (f_c)									
n	7.5	0.71									
	3.75	0.66	0.64								
	3	0.71	0.80	0.53							
	1.5	0.48	0.82	0.45	0.85	0.22					
	0.75	0.94	0.17	0.66	0.88	0.10	0.86	1.1	0.59	0.29	0.16
k	7.5	0.79									
	3.75	0.26	0.28								
	3	-0.2	1.71	-0.13							
	1.5	-1.3	1.90	1.82	0.59	-0.06					
	0.75	0.19	-1.92	2.35	0.05	3.25	0.87	1.98	-0.48	0	1.74

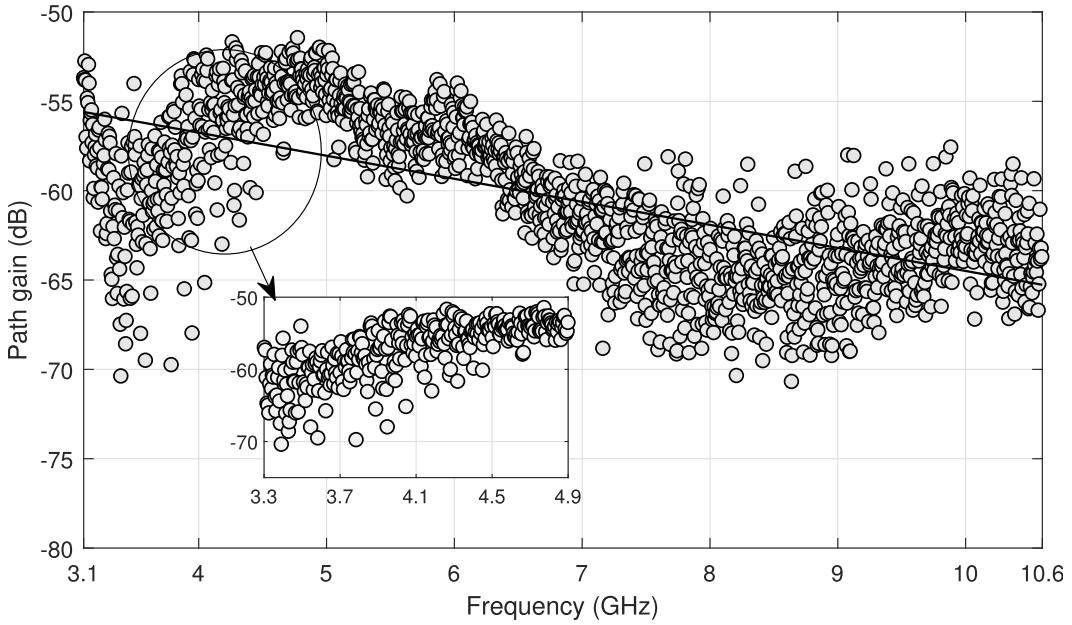

FIGURE 7. Frequency dependent path gain for whole spectrum between Forehead location and UAV.

points and $H(t_i, f_j, d_p)$ is the channel transfer function at a certain time snapshot, frequency tone and distance. For analytical simplicity, the total distance dependent path loss exponent and frequency dependent path loss exponent for a human body is found by averaging the path loss factor (distance and frequency dependent) between the 9 individual body position and the UAV. Fig. 6 shows one such case of estimating distance dependent path loss exponent by linear regression for UWB radio channel between forehead and the UAV. The distance dependent path loss factor n and frequency dependent path loss factor k thus determined for different carrier frequency corresponding to different bandwidths is listed in Table 3. The average value of n varied from 0.1 to 1.1. The general notion for the value of n is that it should be around 2 but since the indoor warehouse environment has metallic surface all around it that thus making the environment perfect for the coherent addition of multipath components at receiver. This in turn results in a small path loss factor values. Similar findings have also been reported in the previous research studies [25], [29].

In contrast, the frequency dependent path loss component has a maximum value of 3.25 and minimum value of -1.92. This shows the frequency dependence of the UWB channel which separates it from the other normal channel models. One may question over the negative k value but on careful observation of Fig. 7 that plots the path gain over the entire spectrum of the UWB channel between Forehead and UAV, it can be observed that the overall trend for the value of k is positive, but for select bandwidths in the spectrum, the value will be negative as shown in the zoomed part of the figure. This is due to the antenna effects such as VSWR, which is frequency dependent (see [23] for detailed antenna specifications). Figs. 8 and 9 show such two cases of positive and negative k at different carrier frequencies corresponding to a given bandwidth in more detail. Therefore, in UWB systems, not only the distance dependent path loss factor but also the frequency dependent path loss factor play a very important role in channel modeling that intrinsically depends on the selected bandwidth and the corresponding carrier frequency. This is a very crucial property to be considered while

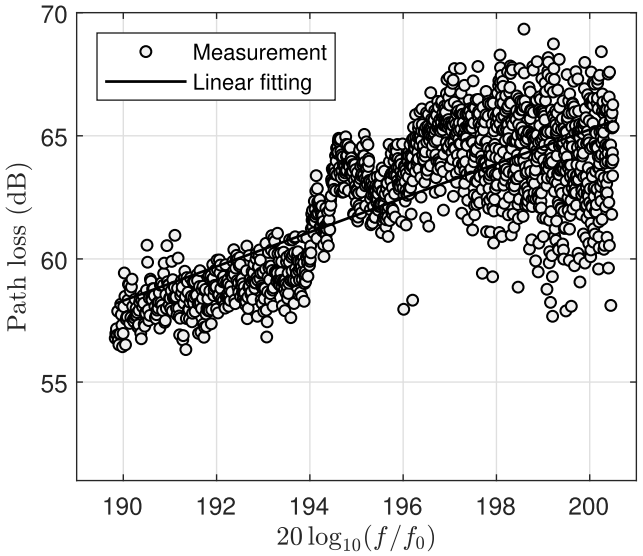

FIGURE 8. Linear fitting to determine the frequency dependent path loss factor (*k*) between Waist location and UAV for the bandwidth of 7.5 GHz with the carrier frequency set at 6.85 GHz.

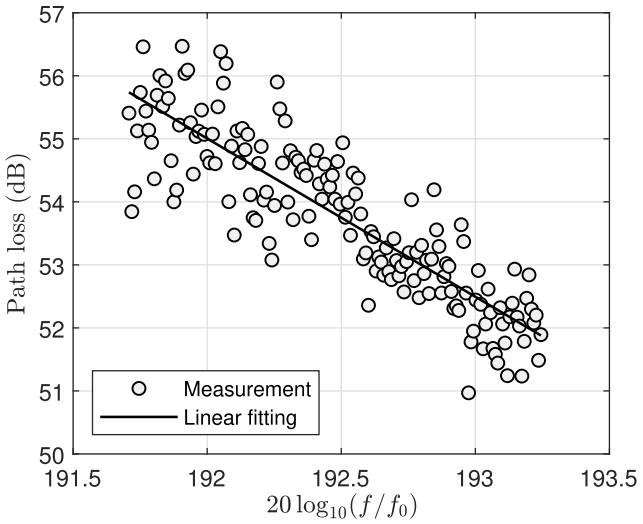

FIGURE 9. Linear fitting to determine the frequency dependent path loss factor (*k*) between Waist location and UAV for the bandwidth of 0.75 GHz with the carrier frequency set at 4.22 GHz.

designing UAV2W systems or UWB systems in general. Now, in the next part, we will look into the time dispersion properties of UAV2W systems.

B. TIME DISPERSION ANALYSIS

Time dispersion parameters using VNA method can be found using discrete time impulse responses. In this method, the multipath delay axis is described by bins that are equally spaced and the resolution of these time bins are determined by the measurement bandwidth. In our setup, the bandwidth was 7.5 GHz (3.1-10.6 GHz), therefore the bin width is 133.3 ps. All the multipath components within a bin are represented by a single multipath component delay. The relative delay

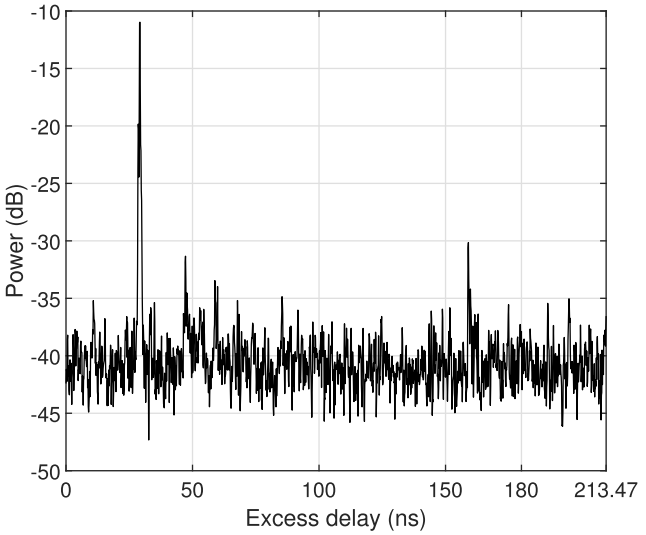

FIGURE 10. PDP for the case of antenna placed at Forehead position where the human subject was at the distance of 8 m from UAV.

between the first arriving path to the maximum resolvable path is known as maximum excess delay. The maximum resolvable path is given by $N\Delta\tau$ where $N = 1601$ is the maximum resolvable path and $\Delta\tau$ is the bin width. Hence, the maximum excess delay in our scenario is 213.47 ns, which can be easily seen in Fig. 10. The measured channel modelled as a time-invariant channel impulse response [25], [26] is given as

$$h(\tau) = \sum_{i=0}^{N-1} \alpha_i(\tau) e^{j\phi(\tau)} \delta(\tau - \tau_i), \tag{5}$$

where $\alpha_i(\tau)$, $\phi(\tau)$, τ_i are the amplitude, phase and excess delay of the i-th multipath component. From the recorded frequency domain VNA channel response ($H(f_i, d_l)$), the time domain response can be found by performing inverse Fourier transform (IFFT) which will yield $h(\tau, d_l)$. Therefore, the power delay profile (PDP) after the IFFT operation is given as,

$$P(\tau, d_l) = |h(\tau, d_l)|^2. \tag{6}$$

The time dispersion parameters such as root mean square delay, mean excess delay, and maximum excess delay depend on this PDP whose threshold in our analysis was set at -15 dB.

The mean excess delay is the first moment of power delay profile and is given as,

$$\bar{\tau} = \frac{\sum_{i=0}^{N-1} \tau_i P(\tau_i)}{\sum_{i=0}^{N-1} P(\tau_i)}. \tag{7}$$

Whereas the root mean square (RMS) delay spread is the second moment of PDP and is given as,

$$\sigma_t = \sqrt{(\tau^2 - \bar{\tau}^2)}, \tag{8}$$

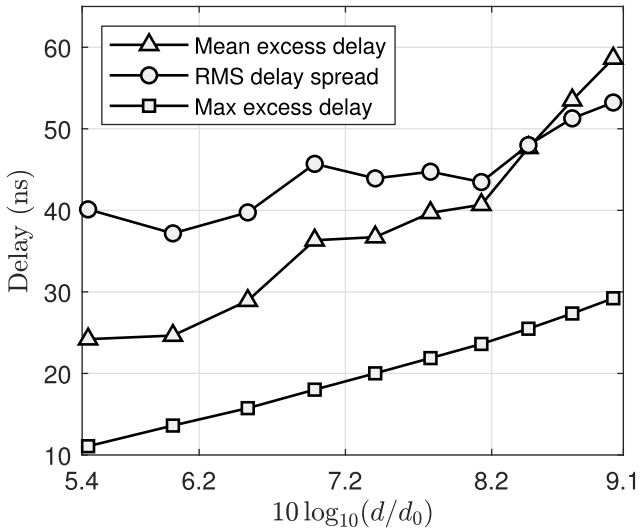

FIGURE 11. Mean excess, maximum excess and RMS delay comparisons with different log distances for antenna located at forehead and PDP threshold set at −15 dB.

TABLE 4. Delay analysis for 9 body locations in case of LOS scenario.

Position	RMS delay (ns)	Mean excess delay (ns)	Maximum excess delay (ns)
Ear	52.82	50.60	23.13
Forehead	46.26	42.77	22.80
Chest	57.17	59.19	27.05
Right Arm	58.83	63.05	24.75
Right Wrist	57.07	62.83	55.63
Waist	60.67	71.1	111.25
Right Thigh	55.31	55.64	39.56
Right Lower Shin	56.37	58.45	40.54
Abdomen	53.83	53.85	24.95
Average	55.37	57.50	41.07

where τ^2 is computed as,

$$\tau^2 = \frac{\sum_{i=0}^{N-1} \tau^2 P(\tau_i)}{\sum_{i=0}^{N-1} P(\tau_i)}. \tag{9}$$

Fig. 10 shows the PDP with delay spread at a distance of 8 m separation from Tx and Rx when the Rx antenna was patched at forehead. Table 4 presents the average value for time dispersion parameters in our LOS warehouse environment. [3] The average value of RMS, mean excess delay and maximum excess delay for our measurement campaign was 55.37 ns, 57.50 ns and 41.07 ns. Although the typical values range from 20 ns to 40 ns but it highly depends on the measurement environment and the set PDP threshold [25], e.g., −15 dB is used in our analysis.

Fig. 11 shows the comparison of maximum excess, mean excess and RMS delay in the case of LOS scenario for the case of Forehead. It can be intuitively observed that as the distance between Tx and Rx increase, so does the RMS, maximum excess and mean excess delays. In next section, we will model the fading statistics of UAV2W systems.

[3]Note that no non-LOS measurements has been considered in this study.

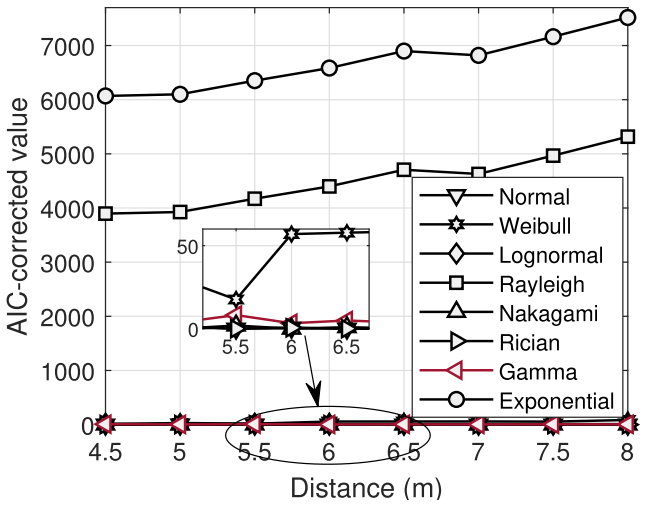

FIGURE 12. AIC test for goodness of fit with different distributions at different distances between the UAV and Forehead position of the human subject.

IV. STATISTICAL MODELING

There has been lot of UWB measurement campaigns where the large scale fading statistics were categorized as Rayleigh, Weibull and Log-normal etc. In our study, as a commonly used model selection test, second order Akaike information criterion (AIC) is used to determine the best fit distribution among these popular distributions [30], [31]. Second order was chosen to take care of different number of parameters in distribution comparison set. For instance, Rayleigh and Exponential are single parameter (rate) distributions, while Weibull has two parameters (shape and scale). Mathematically, this second order AIC is given as [10]:

$$\mathrm{AIC}_c = -2\ln L + 2k + \frac{2k(k+1)}{n-k-1}, \tag{10}$$

where L is the maximized likelihood, k is the number of parameters estimated for that distribution, and n is the number of samples of the experiment. The relative corrected AIC is given as [10],

$$\Delta = \mathrm{AIC}_c - \min(\mathrm{AIC}_c), \tag{11}$$

which implies that zero value will indicate the best fit. The goodness of fit was compared with Normal, Weibull, Log-normal, Rayleigh, Nakagami, Rician, Gamma, and Exponential distributions to determine the best fit distribution.

Based on the results listed in Table 5 and plots from Fig. 12, Log-normal distribution can be easily concluded to be the best fit distribution. The PDF and CDF of a Log-normal distribution is given as,

$$f_X(x) = \frac{1}{\sqrt{2\pi}x\sigma} e^{-\frac{(\ln(x)-\mu)^2}{2\sigma^2}},$$
$$F_X(x) = \frac{1}{2}\mathrm{erfc}\left(-\frac{\ln(x)-\mu}{\sqrt{2}\sigma}\right), \tag{12}$$

where μ and σ are the mean and standard deviation of the Log-normal of a random variable x and erfc(z)

TABLE 5. Comparison of different distributions adopting AIC for nine off-body positions in the indoor environment.

Position	Normal	Weibull	Log-normal	Rayleigh	Nakagami	Rician	Gamma	Exponential
Forehead	10.67	225.97	0.43	5730.87	5.73	10.66	2.47	7935.29
Heart	0.24	46.42	11.34	4501.36	0.91	0.23	5.31	6687.54
Right Wrist	53.22	0.60	104.91	4601.43	67.53	53.31	85.14	6789.21
Abdomen	37.37	4.07	78.53	4732.99	48.44	37.42	62.56	6923.94
Right Thigh	12.58	92.02	35.52	5147.59	18.03	12.60	25.83	7345.34
Right Arm	13.21	38.85	44.98	5838.16	22.32	13.24	32.89	8043.56
Right Shin	15.94	12.95	49.43	4859.50	24.64	15.98	36.16	7052.96
Waist	12.50	163.40	18.84	6019.61	13.29	12.51	15.51	8225.92
Ear	7.61	172.47	16.67	5692.66	9.01	7.61	12.06	7896.93

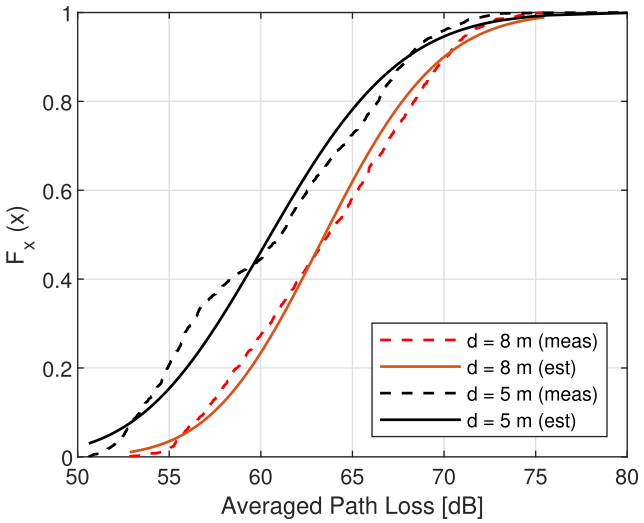

FIGURE 13. Measured and estimated CDF for Forehead off-body radio channel in an indoor environment with the distance between human subject and UAV as 5 and 8 m.

is a complementary error function. Using the estimated Log-normal distribution, the cumulative distribution functions (CDF) at two distances[4] (5 and 7.5 m) are compared with the empirical CDFs (Fig. 13) which also closely matches with each other. This confirms the hypothesis that the fading statistics can be represented by a Log-normal distribution.

V. CONCLUSION

In this paper, a UAV2W system is presented where the different distance dependent and frequency dependent path loss factors are studied and determined in an indoor warehouse environment. Also, the time dispersion characteristics such as root mean square, mean excess delay and maximum excess delay were studied and evaluated accordingly. Finally, using second-order Akakai Information Criteria it was concluded that the fading statistics at ultra-wide band frequencies can be modelled as a Log-normal distribution. This preliminary study of UAV2W will help system designer in link budget calculations for applications of unmanned aerial vehicles in warehouse environment as well as in health care domain.

[4]Only two distances among other measurements are selected for illustrative purposes.

ACKNOWLEDGMENT

The authors would like to thank Dr. James West for his great support and guidance during the measurement campaigns, and Dr. Jamey Jacob's team from Unmanned Systems Research Institute for providing UAVs and pilot support during the measurement campaigns.

REFERENCES

[1] M. Schootman, E. J. Nelson, K. Werner, E. Shacham, M. Elliott, K. Ratnapradipa, M. Lian, and A. McVay, "Emerging technologies to measure neighborhood conditions in public health: Implications for interventions and next steps," *Int. J. Health Geograph.*, vol. 15, no. 1, p. 20, Jun. 2016.

[2] M. J. Lum, J. Rosen, H. King, D. C. Friedman, G. Donlin, G. Sankaranarayanan, B. Harnett, L. Huffman, C. Doarn, T. Broderick, and B. Hannaford, "Telesurgery via unmanned aerial vehicle (UAV) with a field deployable surgical robot," *Stud. Health Technol. Inf.*, vol. 125, pp. 313–315, Feb. 2007.

[3] C. Todd, M. Watfa, Y. El Mouden, S. Sahir, A. Ali, A. Niavarani, A. Lutfi, A. Copiaco, V. Agarwal, K. Afsari, C. Johnathon, O. Okafor, and M. Ayad, "A proposed UAV for indoor patient care," *Technol. Health Care*, pp. 1–8, Sep. 2015.

[4] S. M. Bae, K. H. Han, C. N. Cha, and H. Y. Lee, "Development of inventory checking system based on uav and rfid in open storage yard," in *Proc. Int. Conf. Inf. Sci. Secur. (ICISS)*, Dec. 2016, pp. 1–2.

[5] E. H. C. Harik, F. Guérin, F. Guinand, J. Brethé, and H. Pelvillain, "Towards an autonomous warehouse inventory scheme," in *Proc. IEEE Symp. Ser. Comput. Intell. (SSCI)*, Dec. 2016, pp. 1–8.

[6] M. Fleck, "Usability of lightweight defibrillators for UAV delivery," in *Proc. CHI Conf. Extended Abstr. Hum. Factors Comput. Syst.*, May 2016, pp. 3056–3061.

[7] P. Tatham, F. Stadler, A. Murray, and R. Z. Shaban, "Flying maggots: A smart logistic solution to an enduring medical challenge," *J. Humanitarian Logistics Supply Chain Manage.*, vol. 7, no. 2, pp. 172–193, 2017.

[8] W. G. Patrick, "Request apparatus for delivery of medical support implement by UAV," U.S. Patent 9 307 383, Apr. 5, 2016.

[9] M. M. Khan, Q. H. Abbasi, A. Alomainy, and Y. Hao, "Performance of ultrawideband wireless tags for on-body radio channel characterisation," *Int. J. Antennas Propag.*, vol. 2012, Jun. 2012, Art. no. 232564.

[10] M. M. Khan, Q. H. Abbasi, A. Alomainy, Y. Hao, and C. Parini, "Experimental characterisation of ultra-wideband off-body radio channels considering antenna effects," *IET Microw., Antennas Propag.*, vol. 7, no. 5, pp. 370–380, Apr. 2013.

[11] P. S. Hall and Y. Hao, "Antennas and propagation for body centric communications," in *Proc. 1st Eur. Conf. Antennas Propag.*, Nov. 2006, pp. 1–7.

[12] J. Foerster, E. Green, S. Somayazulu, and D. Leeper, "Ultra-wideband technology for short-or medium-range wireless communications," *Intel Technol. J.*, vol. 2, p. 2001, 2001.

[13] Q. H. Abbasi, M. U. Rehman, K. Qaraqe, and A. Alomainy, *Advances in Body-Centric Wireless Communication: Applications and State-of-the-Art*. Edison, NJ, USA: Institution of Engineering and Technology, 2016.

[14] A. Alomainy, R. Di Bari, Q. H. Abbasi, and Y. Chen, *Co-Operative and Energy Efficient Body Area and Wireless Sensor Networks for Healthcare Applications*. New York, NY, USA: Academic, 2014.

[15] Z. H. Hu, Y. I. Nechayev, P. S. Hall, C. C. Constantinou, and Y. Hao, "Measurements and statistical analysis of on-body channel fading at 2.45 GHz," *IEEE Antennas Wireless Propag. Lett.*, vol. 6, pp. 612–615, 2007.
[16] A. Alomainy, Y. Hao, A. Owadally, C. G. Parini, Y. Nechayev, C. C. Constantinou, and P. S. Hall, "Statistical analysis and performance evaluation for on-body radio propagation with microstrip patch antennas," *IEEE Trans. Antennas Propag.*, vol. 55, no. 1, pp. 245–248, Jan. 2007.
[17] Y. I. Nechayev, Z. H. Hu, and P. S. Hall, "Short-term and long-term fading of on-body transmission channels at 2.45 GHz," in *Proc. Loughborough Antennas Propag. Conf.*, Loughborough, U.K., Nov. 2009, pp. 657–660.
[18] Q. H. Abbasi, A. Sani, A. Alomainy, and Y. Hao, "Arm movements effect on ultra wideband on-body propagation channels and radio systems," in *Proc. Loughborough Antennas Propag. Conf.*, Nov. 2009, pp. 261–264.
[19] Q. H. Abbasi, A. Sani, A. Alomainy, and Y. Hao, "On-body radio channel characterization and system-level modeling for multiband OFDM ultra-wideband body-centric wireless network," *IEEE Trans. Microw. Theory Techn.*, vol. 58, no. 12, pp. 3485–3492, Dec. 2010.
[20] A. Alomainy, Q. H. Abbasi, A. Sani, and Y. Hao, "System-level modelling of optimal ultra wideband body-centric wireless network," in *Proc. Asia–Pacific Microw. Conf.*, Dec. 2009, pp. 2188–2191.
[21] W. Khawaja, I. Guvenc, and D. Matolak, "UWB channel sounding and modeling for UAV air-to-ground propagation channels," in *Proc. IEEE Global Commun. Conf. (GLOBECOM)*, Dec. 2016, pp. 1–7.
[22] J. Tiemann, F. Schweikowski, and C. Wietfeld, "Design of an UWB indoor-positioning system for UAV navigation in GNSS-denied environments," in *Proc. Int. Conf. Indoor Positioning Indoor Navigat. (IPIN)*, Oct. 2015, pp. 1–7.
[23] *Octane Ultra-Wideband Antenna (BW-3000-10000-EG)*. Accessed: Dec. 20, 2018. [Online]. Available: http://www.pharad.com/pdf/UWB-Wearable-Antenna-Datasheet-Enhanced-Gain.pdf
[24] *3DR Drones*. Accessed: Dec. 20, 2018. [Online]. Available: https://3dr.com/products/supported-drones/
[25] C. G. Spiliotopoulos and A. G. Kanatas, "Channel measurements and modelling in a military cargo airplane," *Prog. Electromagn. Res. B*, vol. 26, pp. 69–100, 2010.
[26] A. F. Molisch, "Ultra-wide-band propagation channels," *Proc. IEEE*, vol. 97, no. 2, pp. 353–371, Feb. 2009.
[27] A. F. Molisch, D. Cassioli, C. C. Chong, S. Emami, A. Fort, B. Kannan, J. Karedal, J. Kunisch, H. G. Schantz, K. Siwiak, and M. Z. Win, "A comprehensive standardized model for ultrawideband propagation channels," *IEEE Trans. Antennas Propag.*, vol. 54, no. 11, pp. 3151–3166, Nov. 2006.
[28] C.-C. Chong, Y.-E. Kim, S. K. Yong, and S.-S. Lee, "Statistical characterization of the UWB propagation channel in indoor residential environment," *Wireless Commun. Mobile Comput.*, vol. 5, no. 5, pp. 503–512, 2005.
[29] J. Karedal, S. Wyne, P. Almers, F. Tufvesson, and A. F. Molisch, "A measurement-based statistical model for industrial ultra-wideband channels," *IEEE Trans. Wireless Commun.*, vol. 6, no. 8, pp. 3028–3037, Aug. 2007.
[30] A. Fort, C. Desset, P. De Doncker, P. Wambacq, and L. Van Biesen, "An ultra-wideband body area propagation channel model-from statistics to implementation," *IEEE Trans. Microw. Theory Techn.*, vol. 54, no. 4, pp. 1820–1826, Jun. 2006.
[31] K. P. Burnham and D. R. Anderson, *Model Selection Multimodel Inference: A Practical Information-Theoretic Approach*. New York, NY, USA: Springer, 2003.

AMIT KACHROO (S'14) received the B.Tech. degree in electronics and communications engineering from NIT, Srinagar, India, from 2005 to 2009, and the M.Sc. degree from Istanbul Sehir University, Istanbul, Turkey, from 2015 to 2017. He is currently pursuing the Ph.D. degree in electrical and computer engineering from Oklahoma State University, Stillwater, OK, USA, under the supervision of Dr. S. Ekin. From 2010 to 2014, he was a Project Engineer with Nokia Networks, India, on GSM, WCDMA, LTE, and RF technologies. His research interests are in statistical modeling of wireless channels, statistical learning, machine learning, and cognitive radios. He is also a member of the Honor Society of Phi Kappa Phi.

SURBHI VISHWAKARMA was born in India, in 1993. She received the bachelor's degree from the Vellore Institute of Technology, Vellore, India, and the M.Sc. degree in electrical and computer engineering from Oklahoma State University, in 2018, under the supervision of Dr. S. Ekin. She is currently a Networking Engineer with The Walt Disney Company.

JACOB N. DIXON received the B.S. and M.S. degrees in electrical engineering from Oklahoma State University, in 2015 and 2018, respectively. He was a Research Assistant with Oklahoma State University, from 2015 to 2018. His research topics include unmanned air system communication integrity, environmental studies for communication reliability, spatial sampling and mapping of electromagnetic fields, and applied computational electromagnetics. He is currently an Electromagnetic Compatibility (EMC) Engineer with IBM, Rochester, MI, USA. His current areas of interests include product design for emissions reduction and system immunity, test design for immunity against intentional radiators, and lab automation software development.

HISHAM ABUELLA received the B.Sc. degree in communications and electronics engineering from Ain Shams University, Cairo, Egypt, in 2013. He was a Digital System Design Engineer with Varkon Semiconductor (Wasiela) Company, Cairo, Egypt. In 2014, he joined Istanbul Sehir University as a Research Assistant for his M.Sc. degree in electronics and computer engineering from Istanbul Sehir University, Turkey. Lastly, he joined Oklahoma State University as a Graduate Research Assistant to pursue his Ph.D. degree with the School of Electrical and Computer Engineering, in 2017. He is currently with the Wireless Communications and Sensing Research Lab (WCSRL), under the supervision of Dr. S. Ekin. His current research interests include visible light communication, wireless communication systems design using SDRs, visible light sensing applications, and machine learning and DSP algorithms for wireless communication systems.

ADITHYA POPURI received the B.S. degree in electronics and telecommunication from GITAM University, Bengaluru, India, in 2016, and the M.Sc. degree in electrical and computer engineering from Oklahoma State University, in 2018, under the supervision of Dr. S. Ekin. He is currently with Euclideon, India, as a Smart Experiences Engineer. His research topics include cognitive radio networks and livestock monitoring via the Internet of Things.

QAMMER H. ABBASI (SM'16) received the B.Sc. and M.Sc. degrees (Hons.) in electronics and telecommunication engineering from the University of Engineering and Technology (UET), Lahore, Pakistan, and the Ph.D. degree in electronic and electrical engineering from Queen Mary University of London (QMUL), U.K., in 2012, where he was a Postdoctoral Research Assistant with the Antenna and Electromagnetics Group, in 2012. From 2012 to 2013, he was an International Young Scientist under the National Science Foundation China (NSFC), and an Assistant Professor with the University of Engineering and Technology (UET), Lahore. From 2013 to 2017, he was with the Department of Electrical and Computer Engineering, Centre for Remote Healthcare Technology and Wireless Research Group, Texas A&M University (TAMUQ), initially as an Assistant Research Scientist and was later promoted to an Associate Research Scientist and a Visiting Lecturer, where he was leading multiple Qatar National Research Foundation Grants (worth 3 million dollars). He is currently a Lecturer (Assistant Professor) with the School of Engineering, University of Glasgow, in addition to the Visiting Research Fellow with QMUL and a Visiting Associate Research Scientist with TAMUQ. He has been mentoring several undergraduate, graduate students, and postdocs. He has contributed to a patent, over 220 leading international technical journals and peer-reviewed conference papers, and seven books. His research interests include nano-scale communication, compact antenna design, RF design, and radio propagation, terahertz sensing for plant and human health, RFID, the Internet of Things, antenna interaction with human body, wearables and implants, body centric wireless communication issues, wireless body sensor networks, non-invasive health care solutions, and vertical of 5G. He has been a member of the technical program committees of several IEEE flagship conferences and a Technical Reviewer for several IEEE and top-notch journals. He has received several recognitions for his research, including the URSI Young Scientist Award, the University Research Excellence Award from TAMUQ in two consecutive years, the Reward for Excellence from the University of Glasgow, the UK Exceptional Talent Endorsement (awarded to early career world-leading innovators and scientists) by the Royal Academy of Engineering, the National Talent Award from the Government of Pakistan, National Interest Waiver from USA, most downloaded paper in the IEEE Terahertz Transaction. Media coverage by Analog IC tips, Microwaves & RF newsletters, Vertical news. He is an Associate Editor of IEEE Access, the IEEE Journal of Electromagnetics, the *RF and Microwaves in Medicine and Biology*, the *Journal of Advance Electromagnetics*, and has acted as a Guest Editor for numerous special issues in top notch journals. He has contributed in organizing several IEEE conferences, workshops, and special sessions, in addition to the European school of antenna course.

CHARLES F. BUNTING (F'18) received the A.A.S. degree in electronics technology from the Tidewater Community College, Virginia Beach, VA, USA, in 1985, the B.S. degree in engineering technology from Old Dominion University, Norfolk, VA, USA, in 1989, and the M.S. and Ph.D. degrees in electrical engineering from Virginia Tech, Blacksburg, VA, USA, in 1992 and 1994, respectively.

He was with the Naval Aviation Depot, Norfolk, as an Apprentice, an Electronics Mechanic, and an Electronics Measurement Equipment Mechanic, from 1981 to 1989. From 1994 to 2001, he was an Assistant/Associate Professor with the Department of Engineering Technology, Old Dominion University, where he worked closely with the NASA Langley Research Center on electromagnetic field penetration in aircraft structures and reverberation chamber simulation using finite-element techniques. In 2001, he joined the faculty of Oklahoma State University (OSU), Stillwater, OK, USA, as an Associate Professor and was promoted to a Full Professor, in 2011. In 2012, he was named as the Halliburton Professor of Engineering and the Bellmon Chair (2016). In 2012, he became the Associate Dean of Research of the College of Architecture and Technology. He is the Director of the Robust Electromagnetic Field Testing and Simulation Laboratory, OSU, where he is currently a Professor of electrical and computer engineering. Under his leadership, OSU has become an important center of electromagnetic compatibility (EMC), continuing education for the application of test methodologies for radiated emissions and susceptibility. The reverberation chamber course has been held annually in Stillwater, since 2007, drawing from industry and government, providing engineers with practical training in the application of statistical methods required for proper reverberation chamber operation (over 200 attendees total). His research interests include electromagnetic field penetration in aircraft structures and reverberation chamber simulation using numerical and experimental methods, engineering education, applied computational electromagnetics, statistical electromagnetics, and electromagnetic characterization and application of reverberation chambers for communication systems, including RFID and unmanned aircraft systems (UAS). He has also performed research in the development of near-infrared tomography and microwave acoustic tomography for prostate cancer detection.

Dr. Bunting was a Distinguished Lecturer for the IEEE EMC Society (2011–2012), the IEEE EMC Society Board of Directors (2011–2016), the Technical Activities Committee Vice Chair (2014–2016), and the Vice-President of Technical Services (2017–2021).

JAMEY D. JACOB received the B.S. degree in aerospace engineering from the University of Oklahoma, in 1990, and the M.S. and Ph.D. degrees in mechanical engineering from the University of California at Berkeley, in 1992 and 1995, respectively. He has spent 10 years as a Professor with the Mechanical Engineering Department, University of Kentucky. He is currently the John Hendrix Chair and a Professor with the School Mechanical and Aerospace Engineering and the Director of the Unmanned Systems Research Institute, Oklahoma State University. He is the author of over 100 papers and technical reports in the areas of unmanned systems, aerodynamics, flow control, and inflatable structures. He was a National Research Council Summer Faculty Fellow in the Air Force Research Laboratory at WPAFB, in 2003 and 2004, respectively. He currently serves on the Governor's Aerospace and Autonomous Systems Council and as a President of the Unmanned Systems Alliance of Oklahoma.

SABIT EKIN (M'12) received the B.Sc. degree in electrical and electronics engineering from Eskişehir Osmangazi University, Turkey, in 2006, the M.Sc. degree in electrical engineering from New Mexico Tech, Socorro, NM, USA, in 2008, and the Ph.D. degree in electrical and computer engineering from Texas A&M University, College Station, TX, USA, in 2012. He was a Visiting Research Assistant with the Electrical and Computer Engineering Program, Texas A&M University at Qatar, from 2008 to 2009. In 2012, he was with the Femtocell Interference Management Team in the Corporate Research and Development, New Jersey Research Center, Qualcomm Inc. He joined the School of Electrical and Computer Engineering, Oklahoma State University, Stillwater, OK, USA, as an Assistant Professor, in 2016. He has four years of industrial experience from Qualcomm Inc., as a Senior Modem Systems Engineer with the Department of Qualcomm Mobile Computing. His research interests include the design and performance analysis of wireless communications systems in both theoretical and practical point of views, interference modeling, management and optimization in 5G, mmWave, HetNets, cognitive radio systems and applications, satellite communications, visible light sensing, communications and applications, RF channel modeling, non-contact health monitoring, and the Internet of Things applications. At Qualcomm Inc., he has received numerous Qualstar awards for his achievements/contributions on cellular modem receiver design.